EPJ Appl. Metamat. **9**, 18 (2022)

https://doi.org/10.1051/epjam/2022016

EPJ Applied Metamaterials

Available online at:
epjam.edp-open.org

RESEARCH ARTICLE OPEN ACCESS

Dynamic transmission-reflection dichroism based on humidity-responsive metal-hydrogel-metal nanocavities

Dandan Wang[1,a], Qiang Li[2,a], Yunbin Ying[2], Runhu Li[1], Mingliang Cheng[1], Yingxin Chen[1], Jian Zhang[1,*], and Xuefeng Zhang[1]

[1] International Research Center for EM Metamaterials and Institute of Advanced Magnetic Materials, College of Materials and Environmental Engineering, Hangzhou Dianzi University, Hangzhou 310018, PR China
[2] State Key Laboratory of Modern Optical Instrumentation, College of Optical Science and Engineering, Zhejiang University, Hangzhou 310027, PR China

Received: 22 September 2022 / Accepted: 9 November 2022

Abstract. "Lycurgus cup" effect, referring dichroism between reflection and transmission modes of the same structures, is a peculiar phenomenon of multi-faceted display in structural color. Beyond the static dichrotic display, the realization of dynamic dichroism desires active materials and tunable structures, and owns the great demand from smart display, anti-counterfeiting and environmental sensing. We hereby propose a metal-hydrogel-metal (MHM) nanocavity for dynamic dichrotic display. This structure includes thin silver layers to induce the partial transmission with the existing reflection, and a polyvinyl alcohol (PVA) hydrogel layer owning the swelling/deswelling deformability to humidity change. The following experimental measurements and theoretical analysis prove that the reflection and transmission modes exist at distinct wavelengths, and the swelling hydrogel layer by humidity change between 10 and 90% RH can dynamically modulate the dichrotic resonance with the wavelength shift over 100 nm. Such environmental-sensitive and real-time tunable dichroism with hydrogel-based structural color is then verified for multi-color printing, resolution test, and cycling test.

Keywords: Transmission-reflection dichroism / dynamic structural color / MIM nanocavity / hydrogel microstructure / gray-scale exposure

1 Introduction

In nature, the color camouflage of chameleon skin, the visual stealth of mimic octopuses, and the angle-dependent color rendering of Morphobutterfly wings have always attracted people to explore structural color [1–3]. The current coloration based on synthetic dyes is suffering the disadvantages of environmental pollution, complicated synthetic process, and short lifetime [4–6]. In contrast, structural color shows the superiorities of long-time coloration via interaction between incident light and sub-wavelength structures, programable spectra through designing structural parameters, and high display quality by light diffraction, interference and scattering at aimed wavelength [7].

"Lycurgus cup" effect, showing dichrotic color between reflection and transmission of the same structures, is a peculiar phenomenon in structural color [8,9]. In Lycurgus cup, dispersed Au and Ag colloid nanoparticles cause plasmonic absorption at ~520 nm during light propagation through glass and induce red coloration for transmission mode. Without plasmonic absorption, the light scattering on glass surface leads to green coloration for reflection mode [10]. This dichrotic coloration depending on the location of incident light is also noticed in stained glass on church windows [11]. The dichroism between reflection and transmission enriches the multi-faceted display of structural color [12], and owns unique potential in anti-counterfeiting, smart displays, optical sensing [13–15].

Currently, dichrotic structural color are mainly realized by fabricating periodic nanostructures or randomly dispersing metallic nanoparticles [16–18]. The first approach requires high-precision and large-area nanofabrication techniques to realize sub-wavelength features [19,20], and the process is relatively expensive and time-consuming. The second approach containing random location of metallic nanoparticles is difficult for accurately engineering single-pixel spectrum with high resolution and multicolor display [17,21]. Photonic crystals (PCs) are also utilized for dichrotic structural color, and their band gap controlled by certain thickness and lattice spacing can

* e-mail: jianzhang@hdu.edu.cn
[a] Dandan Wang and Qiang Li contributed equally to this work.

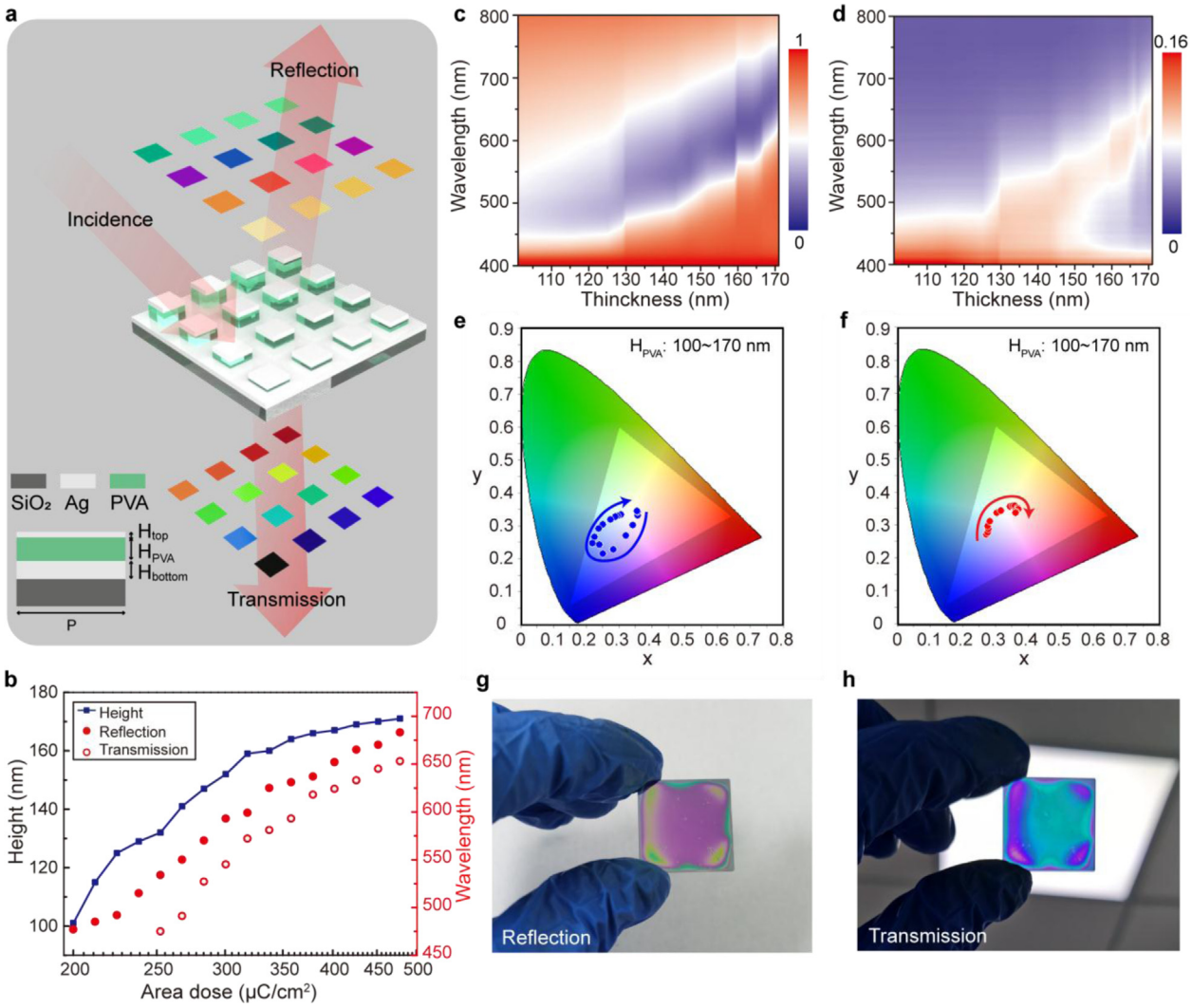

Fig. 1. (a) Schematic of MHM structures displaying dichroism between reflection and transmission modes. The MHM structures contain top Ag layer ($H_{top} = 10$ nm), PVA layer (H_{PVA}: 100–170 nm) and bottom Ag layer ($H_{bottom} = 30$ nm). (b) Height of PVA (the blue line), reflection and transmission resonances (the red dots and red circles respectively) of the corresponding MHM structures fabricated with varied EBL exposure dose. 2D contours of (c) reflection and (d) transmission spectra of MHM structures with the varied H_{PVA} of 100–170 nm. Corresponded 1931CIE diagrams with the varied H_{PVA} of 100–170 nm for (e) reflection and (f) transmission modes, respectively. Photographs of large-area MHM film showing different color for (g) reflection and (h) transmission modes visible to naked eye.

manage the light propagation separately in reflection and transmission modes [22]. PCs coloration relies on the self-assembly of nanospheres, and thus it is challenge in configurably stack nanospheres in micro/nanoscale for multicolor and high-density display.

Despite the multi-faceted display with static dichroism, major efforts are still required for dynamic control of structural color which enables advanced functionalities such as environmental camouflage, secure encryption, optical sensing and solar-energy control [23–26]. The current strategies mainly rely on phase-change materials, such as chalcogenides and vanadium oxide, of which the optical properties can be switched between two distinct phases [27–29]. While, the high extinction coefficient k of phase-change materials hinders the light transmission at visible wavelength range [30]. The transmittance of electrochromic films can also be real-time tuned by applying an external electrical field, though additional design of circuits is needed to integrate the active films with capacitor electrodes [31,32]. What is more, dynamic and high-resolution multicolor display requires configurable 3D-fabrication techniques in nanoscale, and the feasible patterning and etching processes for the inorganic materials are still limited due to their resistant chemical composition [33].

Electron-beam lithography (EBL) is widely used in manufacturing micro-/nanostructures because of its configurable designation, nanoscale resolution and non-mask fabrication process [34]. It has been proved that hydrogel, as one kind of real-time deformable polymer with aqueous stimuli [35,36], can be high-resolution patterned with electron-beam exposure and utilized for dynamic multicolor display by humidity control [37,38]. In this work, we propose a

metal-hydrogel-metal (MHM) structure as dynamic Fabry-Parrot nanocavity for dichrotic structural color, and this structure is composed of the hydrogel as the humidity-responsive insulator layer between two ultra-thin metallic mirrors for multi-layer interference. Polyvinyl alcohol (PVA), a typical hydrogel with negligible extinction coefficient, was gray-scale patterned through EBL, and the resulted multi-level 3D architecture leads the multicolor rendering covering the whole visible wavelength range. The top and bottom metallic layers with the reduced thicknesses induce the partial transmission with the existing reflection of MHM nanocavities, and thus lead dichroism. The following experimental measurements and theoretical analysis prove the dichrotic plasmonic resonance for reflection and transmission modes at distinct wavelengths. The swelling/deswelling responsibility of hydrogel to humidity change is further utilized in our MHM nanocavities for instantaneous resonance change between 390 and 780 nm and dynamic multi-faceted display.

2 Discussion and results

Figure 1a presents the schematic of our proposed MHM structures displaying dichroism between reflection and transmission modes. The scanning electron microscope (SEM) image in Figure S1 shows the proposed MHM nanocavity consisting of top and bottom thin silver (Ag) layers with the respective thickness of 10 nm and 30 nm on a quartz substrate, and PVA hydrogel film as the humidity-responsive insulator layer. Ag is selected as the mirror layers because of its low loss and plasma resonance covering the whole visible range [39]. Visible to naked eye in Figures 1g and 1h, this multi-layer film can directly render distinct color depending on the observation location. The surface flatness of bottom Ag layer, spin-coated PVA layer, top Ag layer are tested successively by atomic force microscope (AFM images in Fig. S2), and the measured Root Mean Square (RMS) of surface roughness for the three layers is 2.98, 0.85 and 2.56 nm, respectively. The smooth surfaces of three layers can benefit the large-area and uniform dichrotic display in the following experiments.

In previous reports, the grayscale-patterning capability of PVA hydrogel as EBL resist was demonstrated, and the height of PVA as the insulator layer can be programmably designed for the aimed resonance of Fabry-Parrot nanocavities [26,38]. Different from the previous works using bottom metallic layer over optical thickness for complete reflection, here we employ the translucent Ag layer with the reduced thickness of 30 nm and realize an additional transmission mode for Fabry-Parrot nanocavities combined with the existing reflection mode. The fabrication process is depicted in Figure S3. The thickness of the PVA hydrogel layer (H_{PVA}) is controlled gradually between 100 and 170 nm by increasing exposure dose between 200 and 500 $\mu C/cm^2$ (Fig. 1b, blue lines), resulting in the shifted resonance of MHM nanocavities for transmission and reflection modes simultaneously (red dots for reflection mode and red circles for reflection mode in Fig. 1b, respectively). With the increasing H_{PVA} from 100 to 170 nm, Figure 1c detailedly shows the redshift of the reflection valley from 477 to 683 nm, while Figure 1d contrastively shows the redshift of the transmission peak from 475 to 693 nm. These changes make the dichroism in 1931CIE diagrams cover different color range of sRGB (the triangular area) for the two modes as shown in Figures 1e and 1f. For the reflection mode, the chromaticity coordinate (x, y) is changed from (0.3264, 0.3265) to (0.309, 0.2702) with H_{PVA} increased from 100 nm to 170 nm, as the arrow marked in Figure 1e. For the transmission mode, the chromaticity coordinate (x, y) is changed from (0.2966, 0.251) to (0.2537, 0.2345) with H_{PVA} increased from 100 nm to 170 nm, as the arrow marked in Figure 1f. It is noticed that the transmission intensity is not as high as the reflection one, which can be explained by the partial absorption from the translucent Ag layer. However, the red shift of transmission peak from 475 to 693 nm is still detectable by gradually increasing PVA thickness, resulting in a visible color change by naked eye. The reflection and transmission of the same initial PVA thickness render different colors, which proves the static dichroism of our proposed MHM structure.

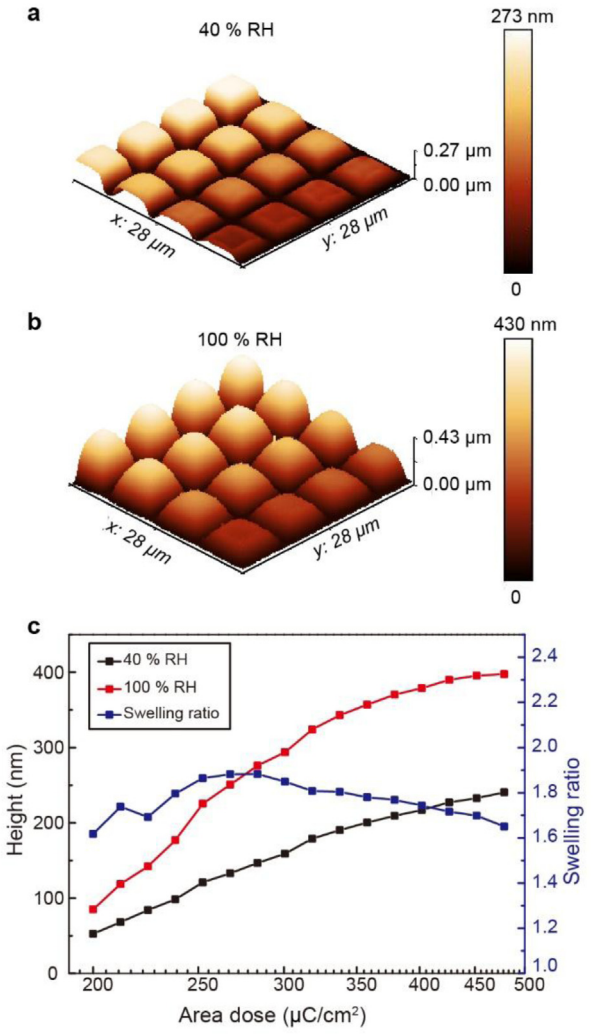

Fig. 2. e-AFM images of hydrogel structures with controlled ambient humidity at (a) 40% RH and (b) 100% RH. (c) Height and calculated swelling ratio of PVA structures exposed with varied dose measured at 40% RH and 100% RH.

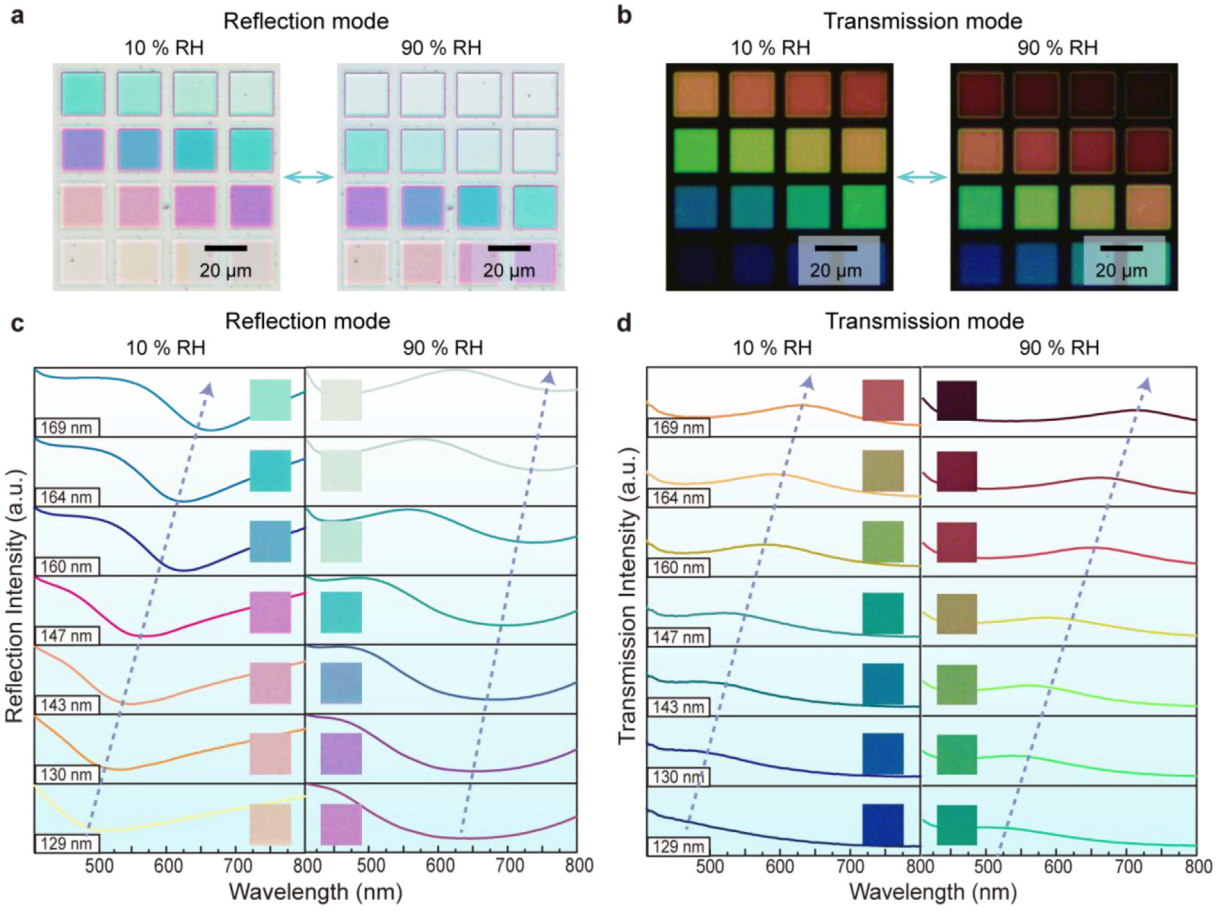

Fig. 3. Dichroitic displays of (a) reflection and (b) transmission modes for the same PVA structures at 10% RH (dry state) and 100% RH (moist state), respectively. (c) Reflection spectra and corresponding color displays at the dry state (left) and the moist state (right). (d) Transmission spectra and corresponding color displays at the dry state (left) and the moist state (right).The initial H_{PVA} in the spectra of (c) and (d) are 129 nm, 130 nm, 143 nm, 147 nm, 160 nm, 164 nm and 169 nm, respectively.

The impact of the top Ag layer on dichrotic structural color is investigated first. We compare MHM nanocavities with varied H_{PVA} as multicolor palettes coated with H_{TOP} of 5 and 10 nm. The color palettes with H_{TOP} of 5 nm lack brightness and contrast for both reflection and transmission modes (Fig. S4a), compared with the samples with H_{TOP} of 10 nm (Fig. S4b). Figure S5 also proves that the full-width-half-maxima (FWHM) of reflection spectra can be improved by increasing H_{TOP} from 5 to 10 nm (i.e. FWHM is reduced from 265 nm to 197 nm for $H_{PVA} = 160$ nm), leading to the higher saturation of structural color in Figure S4b. This is because that a thinner top layer may attenuate the multi-layer interference [40]. Multicolor palettes are also characterized with different ambient humidity of 10 and 90% RH, and both of the samples with H_{TOP} of 5 and 10 nm show the red-shift of the reflection spectra (Fig. S5). A thicker top layer will reduce the transmission and hinder the moisture absorption, as proved in our previous work [38]. Thus, MHM structures with H_{TOP} of 10 nm is conducive for our further study of humidity-tunable dichrotic structural color.

Beyond static multicolor dichroism based on engineering the thickness of hydrogel interlayer, the swelling/deswelling deformability of hydrogel leads to the real-time thickness change of the insulator layer in MHM nanocavities and can further enable the dynamical control of dichrotic structural color. The deformability of PVA structures responding to humidity change is investigated by environmental atomic force microscopy (e-AFM) in this study. The surface morphology of as-exposed PVA structures with varied H_{PVA} was measured with e-AFM at 40 RH % (Fig. 2a), and the fully-swelled PVA structures were measured at 100 RH% (Fig. 2b). By increasing the humidity from 40% RH to 100% RH, H_{PVA} can be enlarged to be 85–397 nm from the initial thickness of 53–240 nm (Fig. 2c). The swelling ratio of PVA (calculated as swelled H_{PVA}/initial H_{PVA}) with varied initial thickness is kept at ~1.8, proving the uniform deformability of patterned PVA structures. Based on this, real-time tunable dichroism of MHM nanocavities covering the visible range can be further realized by controlling ambient humidity as demonstrated in Movie S1, S2 and Figure 3a.

Figures 3 detailedly compares the reflection and transmission spectra measured at 10% RH (named as the dry state) and 90% RH (named as the moist state) with the initial H_{PVA} of 129 nm, 130 nm, 143 nm, 147 nm, 160 nm, 164 nm and 169 nm respectively, and the original

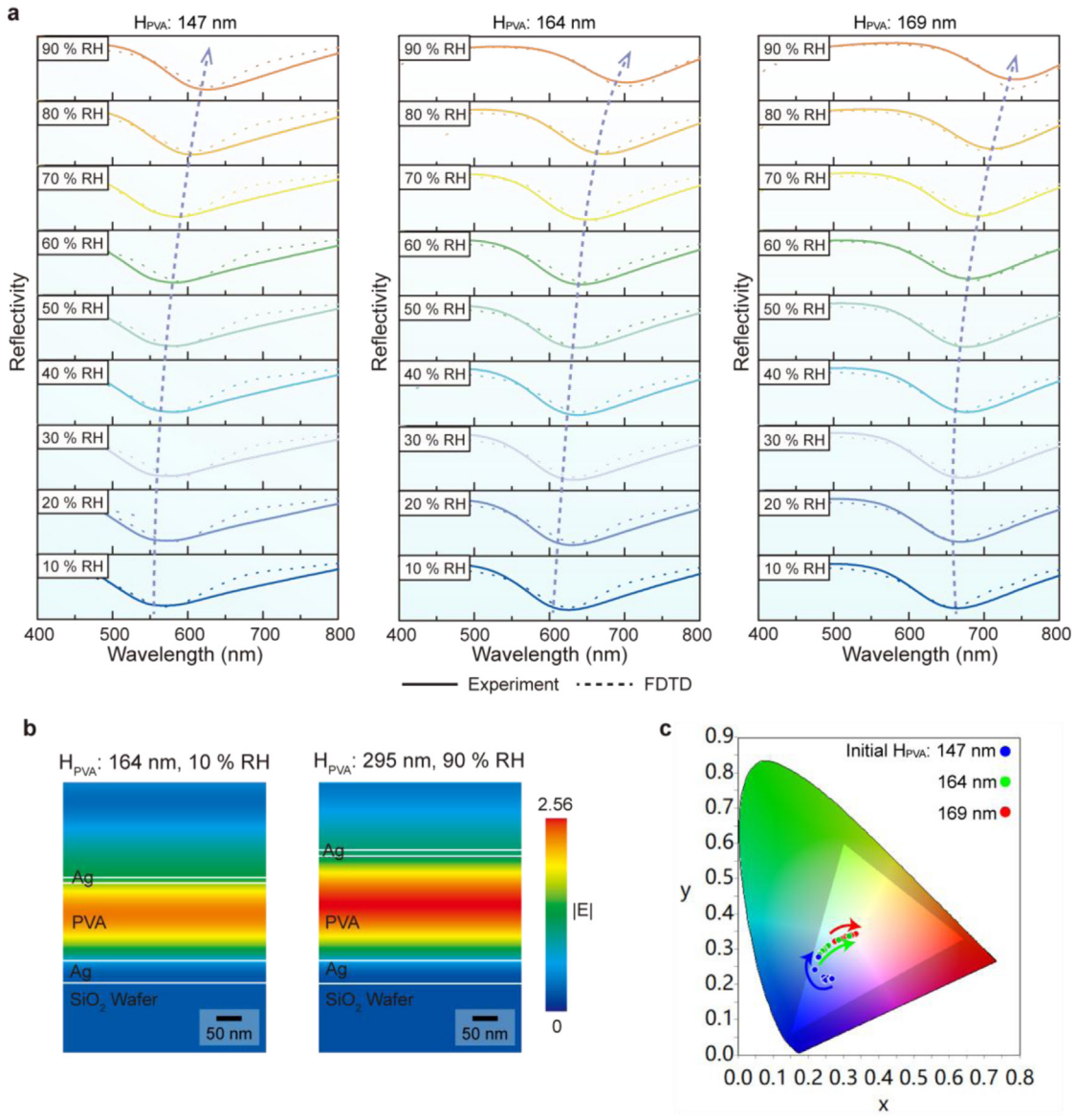

Fig. 4. (a) Experimental and simulated reflection spectra at stepwise increasing ambient humidity from 10 to 90% RH. (b) The simulated electric-field distribution for MHM nanocavity with the initial H_{PVA} of 164 nm at 10% RH and fully-swelled H_{PVA} of 295 nm at 90% RH. (c) CIE 1931 diagram of the real-time color change of MHM nanocavities between 10% and 90% RH. H_{PVA} values for (a) and (c) are selected as 147, 164 and 169 nm, respectively.

reflection and transmission spectra with initial H_{PVA} from 100 nm to 170 nm at the dry state are fully listed in Figure S6. At the dry state, Figure 3c(left) shows that the reflection color of $H_{PVA} = 129$ nm is khaki yellow and shifted to cyan green by increasing H_{PVA} to 169 nm, correspondingly the resonance valley is red-shifted from 508 to 664 nm (Fig. S7a). In contrast, Figure 3b(left) shows that the transmission color at the dry state is dark blue and shifted to pink red (Fig. S7b) by increasing H_{PVA} from 129 to 169 nm, and the corresponding transmission peak is ref-shifted from 470 to 632 nm.

At the moist state, both the transmission and reflection modes exhibit the spectral changes in Figures 3 and S8. The red-shift of the resonances for both the reflection and transmission modes can be as great as 120 nm (Figs. 3c and 3d), and thus an obvious color change is visible to the naked eye (Figs. 3a and 3b, Fig. S9). The reflected chromaticity diagram at the moist state in Figure S9 interestingly shows a wider color gamut than the chromaticity diagram at the dry state (Fig. S7), due to the enlarged thickness difference between different palettes amplified by the swelling ratio of 1.8. As proved in Figure 2, hydrogel structure is highly sensitive to moisture and performs swelling/deswelling deformation to humidity change. Therefore, we demonstrate here that the static multicolor dichroism by MHM nanocavities can be programmed by engineering PVA thickness through gray-scale exposure, and can be further dynamically tuned by controlling the hydrogel swelling to ambient humidity.

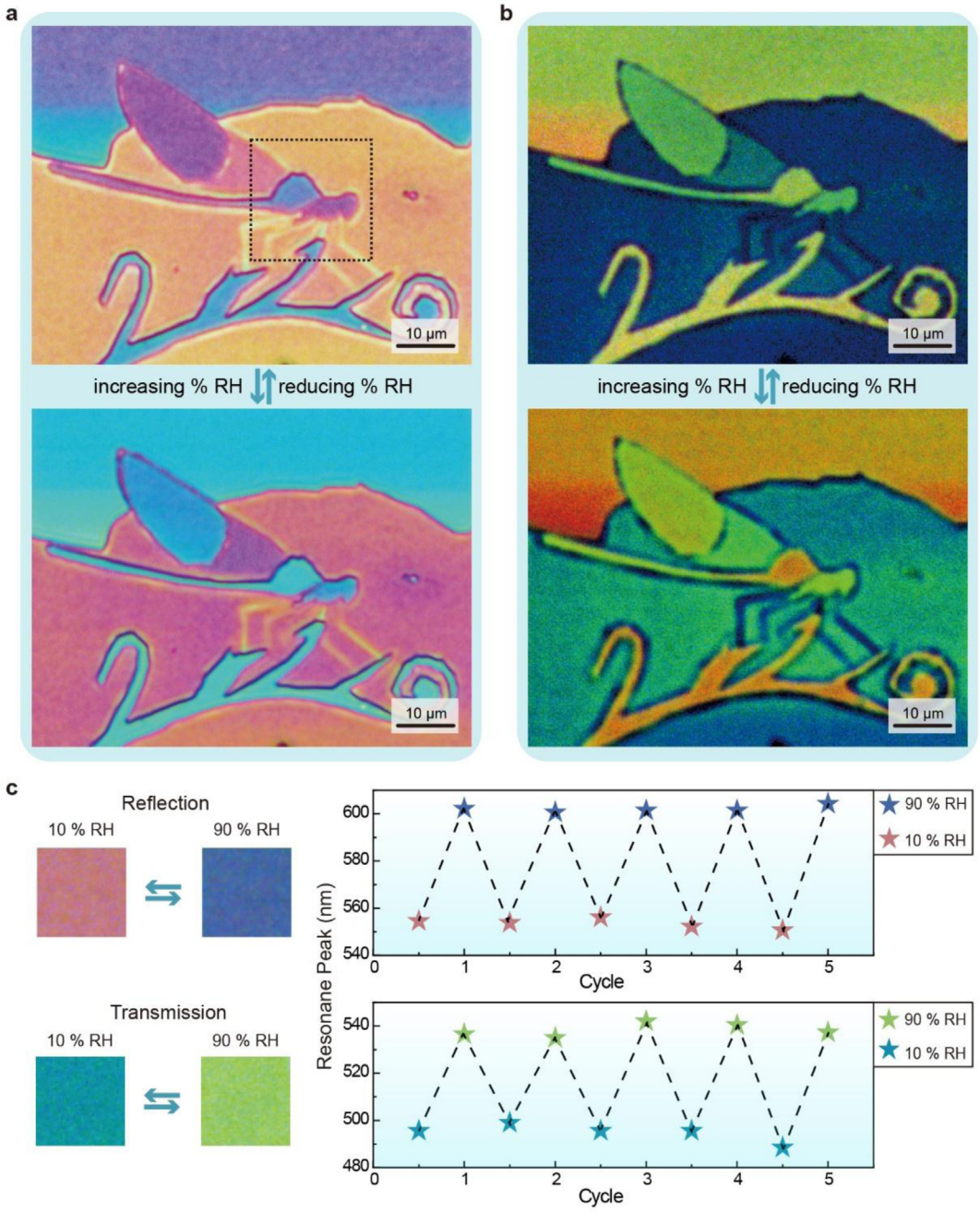

Fig. 5. Dynamic multicolor printing of a dragonfly composed of MIM nanocavities in (a) reflection display and (b) transmission display, reversibly shifted between the dry and moist states.

In order to understand the dynamic dichroism based on MHM nanocavities with swellable hydrogel interlayer, we gradually measure the dichrotic spectra by stepwise increasing the humidity, and numerically calculating the resonance change with different swelling degree in finite-difference-time-domain (FDTD) simulations. We tested the reflection spectra of MHM nanocavities with initial H_{PVA} of 147 nm, 164 nm and 169 nm with varied ambient humidity, respectively (Fig. 4a, solid line). The final swelling ratios of MHM structures at 90% RH with these three H_{PVA} values are set as 1.8 based on Figure 2b. By increasing humidity from 10 to 90% RH, all of the MHM nanocavities with the three original H_{PVA} values show the red-shift gradually from 564 to 627 nm, 623 to 703 nm, and 666 to 742 nm, respectively. When the ambient humidity is lower than 50% RH, the spectral shift is not obvious and the color change is imperceptible. When the ambient humidity is higher than 50% RH, the spectral shift and color change is obvious mainly because the hydrogel interlayer is exposed to sufficient moisture and thus the layer swelling is evident. Correspondingly, we gradually increase the swelling degree of hydrogel layer in simulation and mimic the reflection change. In Figure 4a, the simulated reflection spectra (as shown in dot lines) are

consistent with the experimental results (as shown in solid lines). Figure 4b shows the simulated electric-field distributions of the MHM nanocavities with the initial H_{PVA} of 164 nm at 10% RH and fully-swelled H_{PVA} of 295 nm at 90% RH (calculated with the swelling ratio of 1.8), proving that there is a typical Fabry–Perot resonance maintaining in the nanocavity during the hydrogel layer swelling with humidity change. The measured real-time color change of MHM nanocavities with the initial H_{PVA} of 147 nm, 164 nm and 169 nm are respectively marked in CIE 1931 diagram (Fig. 4c) showing this process of gradual color change by increasing humidity.

By configurably designing MHM nanocavities with varied H_{PVA}, the application of hydrogel-based dichroitic structural color in dynamic multicolor printing is achieved in this work. Figures 5a and 5b are the same photograph of a dragonfly composed of MHM nanocavities with different H_{PVA} which shows dichroitic multicolor display. AFM analysis of the marked area in the center of Figure 5a confirms that the minimum feature size of this printing is 800 nm (Fig. S10). Furthermore, by switching dry and moist states, the dichroitic printing shows distinct color change between reflection and transmission modes according to the humidity change. Resolution is another important issue in high-quality and vivid color generation. We fabricated the pixelated MHM nanocavities with H_{PVA} of 169 nm for three different pixel pitches ($P = 10\,\mu m$, $P = 8\,\mu m$, $P = 5\,\mu m$). The dichroitic color display in reflection and transmission modes are shown in Figure S11, and the two modes show the distinct color difference with the minimum P of 5 μm. Noticed in the transmission mode of Figure S11b, the color of the pixelated patterns with $P = 5\,\mu m$ shifts from red to green. The reason for this change is that the contrast value of PVA hydrogel as the EBL resist is as high as 1.33 [37], leading to a slope sidewall of the pixel and impacting the patterned PVA height and the final multi-layer interference (Fig. S11e).

Finally, we test the reversibility of dichroitic change of our MHM nanocavities by repeating two humidity states of 10 and 90% RH for 5 cycles. The resonance shift, color change and read-time recording spectra for reflection and transmission modes of the MHM nanocavity with the initial H_{PVA} of 143 nm are respectively presented in Figure 5c and Figures S12a and S12b, and the repeatable spectra to humidity change match with each cycle. Considering the oxidation of Ag, the device activity can be kept within 1–2 weeks, and a protecting layer or other metal layer instead of Ag may be employed to improve the device longevity. Based on this, we propose hydrogel-based MHM nanocavities for real-time controllable and reversible dichroism, providing a new solution for multi-faceted multicolor display.

3 Conclusion

Dynamic dichroism between reflection and transmission modes is realized with hydrogel-based MHM nanocavities in this work. The nanocavities employ a humidity-responsive hydrogel interlayer and two mirror metallic layers with reduced thicknesses. The thin metallic layer induces partial transmission besides the existing reflection, and thus the static multicolor dichroism is realized with the gray-scale patterned hydrogel layer. The hydrogel interlayer shows swelling/deswelling response to the change of ambient humidity and further impacts the multilayer interference. As a result, transmission and reflection modes of the MHM nanocavities can be simultaneously modulated by switching the humidity. The gradual red-shift of spectra with stepwise increasing humidity is tested and matches the theoretical calculation. The dynamic multi-color printing, resolution test, and cycling test are conducted for our MHM nanocavities, confirming this real-time controllable, reversible and programmable dichroitic display. We believe that hydrogel-based MHM nanocavities could be applied to dynamic photonic devices, such as real-time gas sensing, smart security labeling, and multi-faceted display.

4 Implications and Influences

This work reports a metal-hydrogel-metal (MHM) nanocavity for dynamic dichrotic display. Compared with other works rely on complicated nanostructures, this concise architecture simply contains a triple-layer structure and the color rendering is directly decided by the layer thickness through multi-layer interference. Thus, this easy-access and high-efficiency strategy for dichroism is promising for further practical applications. By the way, this structural color relies on the self-driven swelling/shrinking deformability of hydrogel layer with the change of environmental humidity. The thickness change of hydrogel layer directly leads the resonance shift of both transmission and reflection modes simultaneously.

The authors gratefully acknowledge the National Key Research and Development Program of China (2019YFE0121700), the National Key Scientific Instrument and Equipment Development Project of China (51927802), the Fundamental Research Funds for the Provincial Universities of Zhejiang (GK219909299001-003), National Natural Science Foundation of China (52272292), the Zhejiang Provincial Key Research and Development Program (2019C01121), and Start-up Program of Hangzhou Dianzi University (KYS385618067). The authors thank the supports from the Key Laboratory of 3D Micro/Nano Fabrication and Characterization of Zhejiang Province and Instrumentation and Service Center for Physical Sciences in Westlake University.

Supplementary material

Supplementary material provided by the authors.

The Supplementary Material is available at https://epjam.edp-open.org/10.1051/epjam/2022016/olm.

References

1. Z. Li, Y. Yin, Creating Chameleon-like Smart Actuators, Matter **1**, 550 (2019)

2. X. Cao, Y. Du, Y. Guo, G. Hu, M. Zhang, L. Wang, J. Zhou, Q. Gao, P. Fischer, J. Wang, S. Stavrakis, A. deMello, Replicating the Cynandra opis Butterfly's Structural Color for Bioinspired Bigrating, Adv. Mater. **34**, e2109161 (2022)
3. J. Zi, X. Yu, Y. Li, X. Hu, C. Xu, X. Wang, X. Liu, R. Fu, Coloration strategies in peacock feathers, Proc. Natl. Acad. Sci. U. S. A. **100**, 12576 (2003)
4. J. Sun, B. Bhushan, T. Jin, Structural coloration in nature, RSC Adv. **3**, 14862 (2013)
5. C. Liu, Z. Fan, Y. Tan, F. Fan, H. Xu, Tunable Structural Color Patterns Based on the Visible-Light-Responsive Dynamic Diselenide Metathesis, Adv Mater. **32**, e1907569 (2020)
6. J.H. Yang, V.E. Babicheva, M.W. Yu, T.C. Lu, T.R. Lin, K.P. Chen, Structural Colors Enabled by Lattice Resonance on Silicon Nitride Metasurfaces, ACS Nano **14**, 5678 (2020)
7. K. Yu, T. Fan, L. Shuai, Z. Di, Biomimetic optical materials: Integration of nature's design for manipulation of light, Mater. Sci. **58**, 825 (2013)
8. A. Drozdov, M. Andreev, M. Kozlov, D. Petukhov, S. Klimonsky, C. Pettinari, Lycurgus cup: the nature of dichroism in a replica glass having similar composition, J. Cult. Herit. **51**, 71 (2021)
9. L. Kool, F. Dekker, A. Bunschoten, G.J. Smales, B.R. Pauw, A.H. Velders, V. Saggiomo, Gold and silver dichroic nanocomposite in the quest for 3D printing the Lycurgus cup, Beilstein J. Nanotech. **11**, 16 (2020)
10. I. Freestone, N. Meeks, M. Sax, C. Higgitt, The Lycurgus Cup-A Roman Nanotechnology, Gold Bull. **40**, 270 (2007)
11. M. Ranjan, G. Austin, H. Anusha, P. Sujin, S. Gulsim, Colorimetric Plasmon Resonance Imaging Using Nano Lycurgus Cup Arrays, Adv. Opt. Mater. **1**, 281 (2013)
12. Z. Yang, Y. Chen, Y. Zhou, Y. Wang, P. Dai, X. Zhu, H. Duan, Microscopic Interference Full-Color Printing Using Grayscale-Patterned Fabry-Perot Resonance Cavities, Adv. Opt. Mater. **5**, 1700029 (2017)
13. J.S. Lee, J.Y. Park, Y.H. Kim, S. Jeon, O. Ouellette, E.H. Sargent, D.H. Kim, J.K. Hyun, Ultrahigh resolution and color gamut with scattering-reducing transmissive pixels, Nat. Commun. **10**, 4782 (2019)
14. J. Guo, Y. Tu, L. Yang, Y. Zhang, L. Wang, B. Wang, Design and Simulation of Active Frequency-selective Metasurface for Full-colour Plasmonic Display, Sci. Rep. **8**, 11778 (2018)
15. W. Hong, Z. Yuan, X. Chen, Structural Color Materials for Optical Anticounterfeiting, Small **16**, e1907626 (2020)
16. H. Wang, X. Wang, C. Yan, H. Zhao, J. Zhang, C. Santschi, O. Martin, Full Color Generation Using Silver Tandem Nanodisks, ACS Nano **11**, 4419 (2017)
17. Y. Kuroiwa, T. Tatsuma, Laser Printing of Translucent Plasmonic Full-Color Images with Transmission-Scattering Dichroism of Silver Nanoparticles, ACS Appl. Nano Mater. **3**, 2472 (2020)
18. K. Saito, T. Tatsuma, Asymmetric Three-Way Plasmonic Color Routers, Adv. Opt. Mater. **3**, 883 (2015)
19. X. Zhu, C. Vannahme, E. Hojlund-Nielsen, N.A. Mortensen, A. Kristensen, Plasmonic colour laser printing, Nat. Nanotechnol. **11**, 325 (2016)
20. T. Xu, Y.K. Wu, X. Luo, L.J. Guo, Plasmonic nanoresonators for high-resolution colour filtering and spectral imaging, Nat. Commun. **1**, 59 (2010)
21. R. Yu, P. Mazumder, N.F. Borrelli, A. Carrilero, D.S. Ghosh, R.A. Maniyara, D. Baker, F.J. García de Abajo, V. Pruneri, Structural Coloring of Glass Using Dewetted Nanoparticles and Ultrathin Films of Metals, ACS Photonics **3**, 1194 (2016)
22. S. Wu, B. Huang, Y. Wu, Z. Meng, S. Zhang, Reflection and Transmission Two-Way Structural Colors, Nanoscale **12**, 11460 (2020)
23. F. Fu, L. Shang, Z. Chen, Y. Yu, Y. Zhao, Bioinspired living structural color hydrogels, Sci. Robot. **3**, eaar8580 (2018)
24. C.I. Aguirre, E. Reguera, A. Stein, Tunable Colors in Opals and Inverse Opal Photonic Crystals, Adv. Funct. Mater. **20**, 2565 (2010)
25. X.H. Li, C. Liu, S.P. Feng, N.X. Fang, Broadband Light Management with Thermochromic Hydrogel Microparticles for Smart Windows, Joule **3**, 290 (2019)
26. Z. Wang, C. Dai, J. Zhang, D. Wang, Y. Shi, X. Wang, G. Zheng, X. Zhang, Z. Li, Real-Time Tunable Nanoprinting-Multiplexing with Simultaneous Meta-Holography Displays by Stepwise Nanocavities, Adv. Funct. Mater. **32**, 2110022 (2021)
27. S. Abdollahramezani, O. Hemmatyar, M. Taghinejad, H. Taghinejad, A. Adibi, Dynamic Hybrid Metasurfaces, Nano Lett. **21**, 1238 (2021)
28. B. Gholipour, A. Karvounis, J. Yin, C. Soci, N.I. Zheludev, Phase-change-driven dielectric-plasmonic transitions in chalcogenide metasurfaces, NPG Asia Mater. **10**, 533 (2018)
29. Z. Xu, H. Luo, H. Zhu, Y. Hong, W. Shen, J. Ding, S. Kaur, P. Ghosh, M. Qiu, Q. Li, Nonvolatile Optically Reconfigurable Radiative Metasurface with Visible Tunability for Anticounterfeiting, Nano Lett. **21**, 5269 (2021)
30. M. Wuttig, H. Bhaskaran, T. Taubner, Phase-change materials for non-volatile photonic applications, Nat. Photonics **11**, 465 (2017)
31. Z. Yan, Z. Zhang, W. Wu, X. Ji, R. Zhao, Floating solid-state thin films with dynamic structural colour, Nat. Nanotechnol. **16**, 795 (2021)
32. Z. Wang, X. Wang, S. Cong, J. Chen, Z. Zhao, Towards full-colour tunability of inorganic electrochromic devices using ultracompact fabry-perot nanocavities, Nat. Commun. **11**, 302 (2020)
33. J. Li, Y. Xia, B. Liu, G. Feng, Z. Song, D. Gao, Z. Xu, W. Wang, Y. Chan, S. Feng, Direct evidence of reactive ion etching induced damages in Ge2Sb2Te5 based on different halogen plasmas, Appl. Surf. Sci. **378**, 163 (2016)
34. Y. Chen, Z. Shu, S. Zhang, P. Zeng, H. Liang, M. Zheng, H. Duan, Sub-10 nm fabrication: methods and applications, Int. J. Extrem. Manuf. **3**, 032002 (2021)
35. Y. Lee, Z. Mousavikhamene, A.K. Amrithanath, S.M. Neidhart, S. Krishnaswamy, G.C. Schatz, T.W. Odom, Programmable Self-Regulation with Wrinkled Hydrogels and Plasmonic Nanoparticle Lattices, Small **18**, 2103865 (2021)
36. C. Jung, S.-J. Kim, J. Jang, J.H. Ko, D. Kim, B. Ko, Y.M. Song, S.-H. Hong, J. Rho, Disordered-nanoparticle–based etalon for ultrafast humidity-responsive colorimetric sensors and anti-counterfeiting displays, Sci. Adv. **8**, eabm8598 (2022)
37. J. Zhang, C. Huang, Y. Chen, H. Wang, Z. Gong, W. Chen, H. Ge, X. Hu, X. Zhang, Polyvinyl alcohol: a high-resolution hydrogel resist for humidity-sensitive micro-/nanostructure, Nanotechnology **31**, 425303 (2020)

38. J. Zhang, D. Wang, Y. Ying, H. Zhou, X. Liu, X. Hu, Y. Chen, Q. Li, X. Zhang, M. Qiu, Grayscale-patterned metal-hydrogel-metal microscavity for dynamic multi-color display, Nanophotonics **10**, 4125 (2021)
39. P. Dai, Y. Wang, X. Zhu, H. Shi, Y. Chen, S. Zhang, W. Yang, Z. Chen, S. Xiao, H. Duan, Transmissive structural color filters using vertically coupled aluminum nanohole/nanodisk array with a triangular-lattice, Nanotechnology **29**, 395202 (2018)
40. Z. Yang, Y. Zhou, Y. Chen, Y. Wang, P. Dai, Z. Zhang, H. Duan, Reflective color filters and monolithic color printing based on asymmetric Fabry–Perot cavities using nickel as a broadband absorber, Adv. Opt. Mater. **4**, 1196 (2016)

Cite this article as: Dandan Wang, Qiang Li, Yunbin Ying, Runhu Li, Mingliang Cheng, Yingxin Chen, Jian Zhang, Xuefeng Zhang, Dynamic transmission-reflection dichroism based on humidity-responsive metal-hydrogel-metal nanocavities, EPJ Appl. Metamat. **9**, 18 (2022)